AFRL-RX-WP-TP-2009-4120

SOLID LUBRICATION OF LASER DEPOSITED CARBON NANOTUBE REINFORCED NICKEL MATRIX NANOCOMPOSITES (PREPRINT)

T.W. Scharf , A. Neira, J.Y. Hwang, J. Tiley, and R. Banerjee

University of North Texas

MARCH 2009

AIR FORCE RESEARCH LABORATORY
MATERIALS AND MANUFACTURING DIRECTORATE
WRIGHT-PATTERSON AIR FORCE BASE, OH 45433-7750
AIR FORCE MATERIEL COMMAND
UNITED STATES AIR FORCE

REPORT DOCUMENTATION PAGE

Form Approved
OMB No. 0704-0188

1. REPORT DATE *(DD-MM-YY)*	2. REPORT TYPE	3. DATES COVERED *(From - To)*
March 2009	Journal Article Preprint	

4. TITLE AND SUBTITLE

SOLID LUBRICATION OF LASER DEPOSITED CARBON NANOTUBE REINFORCED NICKEL MATRIX NANOCOMPOSITES (PREPRINT)

5a. CONTRACT NUMBER
FA8650-08-C-5226

5b. GRANT NUMBER

5c. PROGRAM ELEMENT NUMBER
62102F

6. AUTHOR(S)

T.W. Scharf , A. Neira, J.Y. Hwang, and R. Banerjee (University of North Texas)
J. Tiley (AFRL/RXLMD)

5d. PROJECT NUMBER
4349

5e. TASK NUMBER
20

5f. WORK UNIT NUMBER
LM114100

7. PERFORMING ORGANIZATION NAME(S) AND ADDRESS(ES)

University of North Texas
Denton, TX

Metals Branch (AFRL/RXLMD)
Metals, Ceramics, and NDE Division
Materials and Manufacturing Directorate
Wright-Patterson Air Force Base, OH 45433-7750
Air Force Materiel Command, United States Air Force

8. PERFORMING ORGANIZATION REPORT NUMBER

9. SPONSORING/MONITORING AGENCY NAME(S) AND ADDRESS(ES)

Air Force Research Laboratory
Materials and Manufacturing Directorate
Wright-Patterson Air Force Base, OH 45433-7750
Air Force Materiel Command
United States Air Force

10. SPONSORING/MONITORING AGENCY ACRONYM(S)
AFRL/RXLMD

11. SPONSORING/MONITORING AGENCY REPORT NUMBER(S)
AFRL-RX-WP-TP-2009-4120

12. DISTRIBUTION/AVAILABILITY STATEMENT

Approved for public release; distribution unlimited.

13. SUPPLEMENTARY NOTES

Journal article submitted to *Composites Science Technology*. PAO Case Number: 88 ABW-2009-0055; Clearance Date: 09 Jan 2009. The U.S. Government is joint author of this work and has the right to use, modify, reproduce, release, perform, display, or disclose the work. Paper contains color.

14. ABSTRACT

Nickel (Ni) – multi-walled carbon nanotube (MWCNT) nanocomposites have been processed in a monolithic form using the laser-engineered net shape (LENS™) processing technique. Auger electron spectroscopy maps determined that the nanotubes were well dispersed and bonded in the nickel matrix and no interfacial chemical reaction products were determined in the as-synthesized nanocomposites. Mechanisms of solid lubrication were studied by micro-Raman spectroscopy spatial mapping to determine the formation of tribochemical products due to friction and wear processes. It was determined that the Ni-CNT nanocomposite formed an in situ, low interfacial shear strength graphitic film during sliding, which accounted for its decrease in friction coefficients compared to pure Ni.

15. SUBJECT TERMS

Tribology, friction, wear, solid lubricant, carbon nanotubes, metal nanocomposites, laser engineering net shaping, Auger electron spectroscopy, Raman spectroscopy

16. SECURITY CLASSIFICATION OF:			17. LIMITATION OF ABSTRACT:	18. NUMBER OF PAGES	19a. NAME OF RESPONSIBLE PERSON (Monitor)
a. REPORT	b. ABSTRACT	c. THIS PAGE			Jay Tiley
Unclassified	Unclassified	Unclassified	SAR	22	19b. TELEPHONE NUMBER *(Include Area Code)* N/A

Standard Form 298 (Rev. 8-98)
Prescribed by ANSI Std. Z39-18

Solid Lubrication of Laser Deposited Carbon Nanotube Reinforced Nickel Matrix Nanocomposites

T.W. Scharf [*] [1], A. Neira [1], J.Y. Hwang [1], J. Tiley [2] and R. Banerjee [1]

[1] *Department of Materials Science and Engineering and Center for Advanced Research and Technology, University of North Texas, Denton, Texas, USA*
[2] *Materials and Manufacturing Directorate, Air Force Research Laboratory, WPAFB, OH, USA*

Nickel (Ni) – multi-walled carbon nanotube (MWCNT) nanocomposites have been processed in a monolithic form using the laser-engineered net shape (LENS™) processing technique. Auger electron spectroscopy maps determined that the nanotubes were well dispersed and bonded in the nickel matrix and no interfacial chemical reaction products were determined in the as-synthesized nanocomposites. Mechanisms of solid lubrication were studied by micro-Raman spectroscopy spatial mapping to determine the formation of tribochemical products due to friction and wear processes. It was determined that the Ni-CNT nanocomposite formed an in situ, low interfacial shear strength graphitic film during sliding, which accounted for its decrease in friction coefficients compared to pure Ni.

Keywords: Tribology, friction, wear, solid lubricant, carbon nanotubes, metal nanocomposites, laser engineering net shaping, Auger electron spectroscopy, Raman spectroscopy

1. Introduction

Carbon nanotube (CNT) - metal matrix composites offer attractive properties such as high tensile and flexural strength, stiffness, low friction and increased wear resistance [1-4], and are therefore of interest for potential aerospace applications. In many cases, metal-CNT nanocomposites have not shown promising results due to the difficulties associated with processing, especially in terms of achieving a homogenous distribution of the CNTs. In addition, the issues associated with interfacial reactions between the metal matrix and CNTs have led to controversy in the literature [5,6] and may also influence the mechanical and tribological properties of these nanocomposites. Therefore, a number of recent studies have focused on these aspects of metal-CNT nanocomposite processing and characterization of interfaces. We have recently determined using high resolution transmission electron microscopy that the Ni-CNT

*Corresponding Author

interface is well bonded without the presence of any significant interfacial reaction products [7,8]. The Ni-CNT nanocomposites were processed using the laser engineered net shaping (LENS™) technique, which has the advantages of obtaining bulk metal-CNT nanocomposites without significant damage to the CNTs, thus abating the limitation of large-scale production inherent in other techniques such as molecular level mixing, and being a liquid-based processing route, it does not suffer from some of the disadvantages inherent in conventional powder processing techniques, such as enhanced porosity. In addition, the LENS™ process can also be used for depositing functionally graded materials [9,10].

In regard to tribological behavior, it has been shown that the addition of CNTs in polymer [11,12], ceramic [13-16] and metal [4,17-22] matrices results in reduced friction coefficients and wear rates. For example in Cu-CNT composites [4,17,18,21], scanning electron microscopy (SEM) revealed that structural modification of the composite had occurred due to CNTs being present at the tribological interface, however, no tribochemical (chemistry induced by sliding) information of the CNT in the metal was provided to account for the improved tribological properties. In a similar study, the sliding friction behavior of nanocrystalline Ni-CNT composites were tested in ambient conditions and it was determined that less plastic deformation and brittle fracture occurred for the nanocrystalline Ni-CNT composite in comparison to pure nanocrystalline Ni [22]. Most of the research on CNT nanocomposites has emphasized processing/property relationships, such as the role of processing parameters and volume percent of CNT in the matrix to achieve low friction and low wear. While such studies are important for designing improved nanocomposites, both tribochemical and structural modification studies are needed to explain the friction and wear behavior. In particular, there is an obvious contradiction between CNT nanocomposites' mechanical and tribological properties and the traditional model for low-friction coating [23] that associates low friction with low shear strength materials like graphite, not improved hardness materials like CNT-reinforced metals.

An alternative model of friction and wear, introduced by Godet, coworkers and others [24-27], involves third body processes. Third bodies are formed by the relative motion of the two parent (first body) materials in the sliding contact. They often appear first as thin films either transferred to the stationary counterface or spread across the wear track, and then evolve into wear particles. By separating the two first bodies, third bodies take on the chore of transmitting stresses and accommodate the relative motion between the counterfaces. Thus friction and wear behavior is controlled by the third body processes, as opposed to the first body properties. These third bodies, or transfer films, often form *in situ* (during sliding) and may be chemically different than the two first bodies, thus forming a tribochemical phase.

The purpose of the present study is to identify the role of third bodies in the friction and wear behavior of LENS™ deposited Ni-CNT nanocomposites. The approach was to determine

if *in situ* formation of solid lubricating films in humid environments enhance the friction and wear behavior, and the feasibility to generate solid lubricants through microstructural control at the nanometer level. In addition, the presence of different active tribochemical phases present at the sliding interface in controlling the friction and wear behavior will be reported. An underutilized, advanced characterization technique, micro-Raman spectroscopy spatial chemical mapping, was employed for site specific wear studies to elucidate the solid lubrication mechanisms. If metal-CNT nanocomposites are to be utilized in moving mechanical assembly applications that involve sliding and/or rolling contacts, mechanistic studies are necessary to understand the role of tribochemistry and structural evolution.

2. Experimental Details

Similar to rapid prototyping technologies such as stereolithography, the LENS™ process begins with a CAD design file, which is post-processed into a series of 2D layers. The LENS™ unit used for these depositions is manufactured by Optomec, Inc. The substrate was a ¼" inch of thickness 440C stainless steel (SS) and the deposited composites had a square geometry in order to assure a uniform laser heat distribution during the process. To provide the best build, each successive layer is deposited in a scan direction that is different from the previous layer to ensure homogeneity. A high powdered pulsed Nd:YAG laser (power rating of 500 W), emitting near-infrared laser radiation at a wavelength of 1.064 μm, is focused on the substrate to create a melt pool into which the powder feedstock is delivered through an inert gas flowing through a multi-nozzle assembly. The system specific control parameters included laser power of 400 W (35 Amp current), hatch width of 0.25", layer thickness of 0.01", and mass flow rate of Ar in the powder feeders of 3.5 litres/min. The powders used in this study consisted of commercially pure Nickel (44 – 149 μm particle size from Crucible Research^{TM}) and 10 vol% MWCNT (for the Ni + MWCNT nanocomposites). The MWCNTs were processed by standard chemical vapor deposition (CVD)-based techniques and their purity was ~90%. Since the MWCNTs used in this study were in the form of agglomerated particles consisting of multiple nanotubes, it is rather difficult to determine the exact length of these nanotubes, even from transmission electron microscopy (TEM) studies. Nevertheless, based on TEM observations of a few individual nanotubes which had separated from the bundles, the average length was found to be ~10 μm [7,8]. The bundle size (or diameter) of the CNTs before processing was in the range of 5–50 μm. Prior to deposition, the nickel and CNT powders were pre-mixed in a twin-roller mixer consisting of two rolls rotating in opposite directions (one clockwise and one anticlockwise). This mixing was carried out for 24 h, immediately following which the pre-mixed powder was introduced into the power feeder of the LENS™ deposition system and the composites were

laser deposited. The Ni + CNT nanocomposites were LENS™ deposited in a cylindrical geometry of diameter ~10 mm and height ~10 mm.

After deposition, the LENS™ deposited samples were sectioned using an abrasive cutting wheel and subsequently mounted and mechanically polished for metallographic observation. Scanning electron microscopy (SEM) and Auger electron spectroscopy (AES) were performed with a PHI 700 scanning Auger nanoprobe operating at 20 kV and 10 nA. In addition, site-specific micro Raman spectroscopy was carried out in spot and mapping modes using a Thermo Electron Almega XR Dispersive Raman Spectrometer with ~1 μm spot size and 532 nm excitation wavelength. Raman spectra were obtained at a low power of 20 mW corresponding to a laser power density (~25 mW/μm^2); at this power density, no changes in the spectra due to laser surface heating could be seen. The acquisition times were 10 seconds/spectrum with 4 total accumulations taken to average each spectrum. Raman shifts were measured over a frequency range from 200 to 2000 cm^{-1}, with ~2 cm^{-1} resolution. Area maps were acquired by taking measurements at every 5x5 μm spacing.

Friction and wear testing was conducted with a Falex (Implant Sciences) ISC-200 pin-on-disk (POD) system at room temperature. The samples were openly exposed in lab air (~40% RH) during the tests. Tests were performed under a 0.2 or 0.5 N normal load with a 1.6 mm radius 440C SS or Si_3N_4 ball, which correspond to an initial maximum Hertzian contact stress (P_{max}) of ~0.6 or 0.8 GPa, respectively. The sliding speed was fixed at 50 mm/sec. The ratio of tangential to normal load is the coefficient of friction (COF). Friction and wear tests were run out to 10,000 unidirectional cycles. At least three POD tests were performed for each experimental condition. After tribological testing, the wear surfaces were analyzed with optical microscopy and Raman spectroscopy.

3. Results and Discussion

3.1 As-synthesized Nanocomposite (Ni-CNT interface)

Figure 1 shows a representative SEM image in (a) and corresponding AES map in (b) of the as-synthesized Ni-CNT nanocomposite. It is evident that the CNTs are well dispersed in the nickel matrix with a bundle size ranging from ~1 to 3 μm. The high shear stresses during ball milling cause disintegration of CNTs into smaller bundles that physically adhere to the surface of nickel powder particles [8]. This coupled with the instantaneous melting and deposition of the nickel powders results in a homogeneous distribution of CNT bundles within the nickel matrix. The homogeneous distribution and reasonably refined near-spherical carbon-rich regions inside the nickel matrix are clear evidence of the advantage of dry uniform mixing via ball milling,

overcoming the limitations associated with the density difference between nickel and CNT powders. Higher magnification SEM and AES maps of the Ni-CNT interface are shown in Figure 2. From the SEM image in Figure 2(a), the bundle appears to be an agglomerate of randomly oriented CNTs, which indicates that no significant morphological transformation of the CNT bundles occurred during laser deposition. The presence of CNTs in these regions clearly indicates their survivability at high temperatures during melt processing. High temperature thermal stability of CNTs, compared to graphite in nickel matrix [7], permits the CNTs to retain their chemical identity even after being melt processed. However it is difficult to confirm this based on energy dispersive spectroscopy (EDS) analysis inside the SEM, and thus higher spatial resolution AES maps of C, Ni and O maps were performed to identify the chemistry of the bundles. Furthermore, EDS has poor chemical sensitivity to low atomic number elements such as carbon and oxygen. Figures 2(b) and (c) show the Ni and C AES maps, respectively, of the Ni-CNT interface. The brighter areas correspond to a higher magnitude of the selected constituent. Clearly there is a sharp chemical interface between the Ni matrix and CNT bundle and they appear to be well bonded with no evidence of CNT pullout as a result of polishing or damage during the laser deposition process. Figure 2(d) shows the O AES map that indicates initial evidence that there was some surface oxidization of the CNT. Further analysis showed that there was a minor amount of residual SiO_2 and Al_2O_3, from the polishing slurry, present on the CNT surface; the Si and Al AES maps are not shown. Specifically, the brighter, elongated particle on the CNT surface in Figure 2(d) corresponds to a SiO_2 particle while the other oxygen present is from Al_2O_3. From these AES maps, there was no evidence of any interfacial chemical reaction products in the as-synthesized Ni-CNT nanocomposites, which indicates the CNTs have good wettability for molten nickel. This is corroborated by previous TEM results that showed neither an inter-diffused region nor the formation of any interfacial reaction or compound layer, e.g. metastable NiC, at the interface which suggests that the CNTs do not react to any substantial extent with the molten nickel during the laser deposition process [7,8].

3.2 Friction and Wear Behavior

Representative COF versus cycle curves for the Ni-CNT nanocomposites and reference pure Ni is shown in Figure 3. The samples were either tested against a 440C SS, in Figure 3(a), or Si_3N_4, in Figure 3(b) counterface. This allows for a variation in contact stress and metal-on-metal matrix and ceramic-on-metal matrix sliding contacts. It is well known that adhesive forces for like-on-like contacts can result in a higher adhesive component of friction and harder counterfaces, like Si_3N_4, can result in pull-out of the reinforcing phase in the composite [28]. For the latter case, a LENS™ deposited TiB reinforced Ti-Nb–Zr–Ta alloy composite was tested

in sliding against Si_3N_4 and exhibited TiB precipitate pull-out from the softer β-Ti matrix, which resulted in an increased amount of third body abrasive wear [28]. This was circumvented by using a softer 440C SS counterface. A similar study was performed here for the Ni-CNT nanocomposites to determine if the there was CNT pull-out and, if so, its role in the friction and wear processes. From Figure 3, it is clear that the CNTs in the nanocomposite were beneficial in reducing the COF against both counterfaces with respect to the pure Ni deposited sample for the entire 10,000 cycles. Therefore, this COF reduction of ~0.1 against Si_3N_4 and ~0.17 against 440C SS was due to the CNTs. The lowering of friction with CNTs agrees with previous reports for Ni-P [18], Cu [4,17,18,21], and nanocrystalline Ni matrices [22]. The COF values in Figure 3 are also in agreement with Cu-CNT composites at a similar loading of 10 vol% CNT [4]. In addition, it appears that increasing the initial maximum contact stress from 0.6 (Figure 3(a)) to 0.8 GPa (Figure 3(b)) resulted in increasing friction. However, caution must be taken since the specific wear mechanism, e.g. metal oxidative wear and/or adhesive wear, can not be ascribed without examining the structural modification and tribochemical film formation inside the wear tracks. Much of the current literature speculates on their role in controlling the friction and wear processes of metal-CNT composites, and this is the subject of the following section.

3.3 Structural Modification and Tribochemical Reactions

Raman spectroscopy mapping inside the wear tracks was performed to elucidate the mechanisms responsible for the solid lubrication processes. Figure 4 shows Raman spectroscopy color maps overlaid on the optical microscopy images of inside the wear tracks after the two tests shown in Figure 3(a) were stopped at cycle 10,000. These blended images of the optical micrograph and Raman intensity map allow for accurate analysis of what tribochemical products may have formed inside the wear tracks. The blended image for 440C SS counterface sliding against pure Ni and Ni-CNT nanocomposite are shown in Figure 4(a) and in Figure 4(c), respectively. The color scheme shows were the highest intensity (concentration) is of the selected species. For example, the Fe_3O_4 (magnetite [29,30]) Raman peak at 676 cm^{-1} shown in Figure 4(b) for pure Ni was used to generate the color map and its relative intensity scale bar is shown between Figure 4(a) and Figure 4(b). It is apparent that in Figure 4(b) more Fe_3O_4 (peaks at 538 and 676 cm^{-1}) is present inside the wear track (e.g., red circle in Figure 4(a)) than outside the wear track (e.g., blue circle in Figure 4(a)). A similar color map is obtained for the other Fe_3O_4 peak at 538 cm^{-1}. Outside the wear track there is no evidence of any oxide or any other peak from the blue colored Raman spectrum in Figure 4(b). The presence of Fe_3O_4 inside the track is due wear of the 440C SS counterface, despite its higher hardness (Vickers micro hardness of 650) than the pure Ni sample (Vickers micro hardness of 170). The 440C SS

counterface, not shown, did exhibit a small flat which is not surprising since no protective third body (transfer film) formed to protect it from cyclic wear. In addition, the Raman wear map in Figure 4(a) shows evidence of preferential regions of wear inside the track in which there is no, or minimal, Fe_3O_4 present. This is due to the contact area not being homogenous, or fully established, across the interface.

Conversely, the highest intensity (concentration) of tribochemical species inside the wear track in Figures 4(c) and 4(d) for the Ni-CNT nanocomposite are ascribed to the well known carbon D (1347 cm^{-1}) and G (1602 cm^{-1}) peaks, e.g., representative location shown by red circle in Figure 4(c). The D peak origin is due to the breathing modes of sp^2 bonded atoms in rings, the G peak is attributed to the in-plane bond stretching of all pairs of sp^2 bonded atoms in both rings and chains [31,32]. Compared to the G peak at 1582 cm^{-1} for the unworn Ni-CNT nanocomposite (representative location shown by blue circle in Figure 4(c)), the G peak shifted 20 cm^{-1} towards higher wave number, which qualitatively indicates increased graphitization due to the sliding wear process. This is also supported by the increase in ratio of intensities (I_D/I_G) which is a measure of the degree of structural disorder/modification [33] and indicative of increased graphitization [32]. Furthermore, the position of the D peak at 1350 cm^{-1} has not significantly shifted, but instead the full width at half maximum (FWHM) of it and the G peak increase, which indicates that the structurally modified layer exhibits a disordered graphite structure. The unworn Ni-CNT nanocomposite also exhibits a very small shoulder to the G peak, known as the D´ peak located at 1621 cm^{-1}, which is a double-resonance Raman band induced by defects in CNTs [7,8,31]. This CNT D´ peak is no longer present due to the sliding induced graphitization process. Figure 4(d) also shows the reference spectrum for the raw MWCNT powder used as a feedstock for the LENS™ deposition. Its primary peak positions are similar to that of the unworn CNTs in the Ni matrix, however, the unworn Ni-CNT nanocomposite I_D/I_G ratio increased since the degree of graphitization of the MWCNT bundles as well as their defect density increased during laser deposition [7]. Lastly, there is either no Fe_3O_4 or a minimal amount (intensity) in the wear track, not shown, that scales with the wear-induced changes in the graphitic peaks. This indicates that there was still some 440C SS ball wear but not nearly as much as in the pure Ni sample in Figure 4(a).

A similar series of Raman spectroscopy color maps overlaid on the optical microscopy images were generated inside the wear tracks for the Si_3N_4 counterface sliding against pure Ni, in Figure 5(a), and Ni-CNT nanocomposite, in Figure 5(c), for the tribological tests shown in Figure 3(b). The blended image shown in Figure 5(a) for pure Ni was generated by selecting the Raman peak at 553 cm^{-1} inside the wear track which is NiO [34]. Unlike the 440C SS counterface which showed transfer of Fe_3O_4 into the wear track, the harder Si_3N_4 counterface did not exhibit wear since there was no SiO_2 in the wear track and no optical microscopy evidence of

a wear-induced flat. This suggest that the pure Ni sample exhibited oxidation wear, or tribooxidation, since NiO was relatively throughout the wear track (representative location shown by red circle in Figure 5(a)), and not present outside the wear track (representative location shown by blue circle and spectrum in Figures 5(a) and 5(b), respectively). Concomitantly, it is also likely that the heat generated during dry sliding wear resulted in an increase in the interfacial flash temperature between the Si_3N_4 counterface and pure Ni sample, which subsequently would result in the formation of a NiO film, a thermo-oxidation process. A similar tribochemical reaction was determined to occur in Cu-CNT composites where the wear particles extruded from the tracks were identified by x-ray diffraction to be CuO and Cu_2O phases [4].

The Raman spectroscopy color map and spectra of Si_3N_4 counterface sliding against Ni-CNT nanocomposite are shown in Figures 5(c) and 5(d), respectively. Similar to the spatial map and spectra shown in Figures 4(c) and 4(d), the highest intensity (concentration) of tribochemical species inside the wear track are ascribed to the carbon D (1345 cm^{-1}) and G (1604 cm^{-1}) peaks, e.g., representative location shown by red circle in Figure 5(c). Compared to the G peak at 1582 cm^{-1} for the unworn Ni-CNT nanocomposite (representative location shown by blue circle and spectrum in Figures 5(c) and 5(d), respectively), the G peak shifted 22 cm^{-1} towards higher wave number, the I_D/I_G ratio and FWHM of the D and G peaks increased, which all indicate increased graphitization due to the sliding wear process. In addition, there is either no NiO or a minimal amount (intensity) in the wear track, not shown, that also scaled with the wear-induced changes in the graphitic peaks. The wear-induced graphitic film was much more prevalent across the entire wear track as shown in Figure 5(c). This indicates that there is a competition of the graphitic film on the wear track because oxygen would react with the carbon first instead of the nickel matrix because carbon is easier to oxidize than nickel and thus impede NiO formation. As a result, the graphitic film not only provides solid lubrication during sliding, but also prevents the nickel from oxidation. The Si_3N_4 counterface also showed transfer film formation (adhesive wear) with identical Raman D and G peak graphitization parameters as the wear track. This in situ formed, self-mated graphitic film resulted in lower interfacial shear strength, which accounted for the Ni-CNT nanocomposite decrease in friction coefficient compared to pure Ni that oxidized. It has been shown from SEM imaging that a carbon film did not cover the entire wear track in a Cu-CNT composite when the CNT content is low (~8 vol%), but when the CNT volume fraction increased, the carbon film did cover the entire wear track, and impeded oxidation, which is similar to our Ni-CNT nanocomposite loading of 10 vol% [4]. However, it was further determined that when the CNT content is higher than 12 vol%, there were no improvements in wear since there was already sufficient carbon covering the wear track [4]. Lastly, the tribological behavior of the Ni-CNT nanocomposite was not affected due to the

aforementioned minor remnants of SiO_2 and Al_2O_3 from the polishing slurry (Figure 2), since their Raman phases were not present inside the wear track.

4. Conclusions

A homogeneous distribution of CNT bundles in a nickel matrix, without any evidence of debonding or interfacial reaction products, has been determined for a laser deposited Ni-CNT nanocomposite. The mechanisms of solid lubrication in the Ni-CNT nanocomposite were studied by micro-Raman spectroscopy spatial mapping which detected the formation of an in situ wear-induced, low interfacial shear strength graphitic film. This accounted for a decrease in friction coefficient compared to the laser deposited pure Ni which oxidized to form a high shear strength, high friction NiO phase during wear (tribo-oxidation) as determined by Raman spectroscopy in the wear track. These tribochemical products formed are a result of third body processes.

Acknowledgments

This work was supported under the Institute for Science and Engineering Simulation (ISES). The authors would also like to acknowledge the US Air Force Office of Scientific Research (AFOSR Grant No. FA9550-06-1-0193) for providing financial support.

References

[1] S.I. Cha, K.T. Kim, S.N. Arshad, C.B. Mo, S.H. Hong, Adv. Mater. 17 (2005) 1377.
[2] T. Laha, S. Kuchibhatla, S. Seal, W. Li, A. Agarwal, Acta Mater. 55 (2007) 1059.
[3] S. Yamanaka, A. Kawasaki, H. Sakamoto, Y. Mekuchi, M. Kuno, T. Tsukada, J. Jpn. Inst. Met. 70 (2006) 630.
[4] S.R. Dong, J.P. Tu, X.B. Zhang, Mat. Sci. Eng. A 313 (2001) 83.
[5] L. Ci, Z. Ryu, N.Y. Jin-Phillip, M. Rühle, Acta Mater. 54 (2006) 5367.
[6] D. Chunfeng, Z. Xuexi, W. Dezun, Mater. Lett. 61 (2007) 904.
[7] J. Y. Hwang, A. Neira, T. W. Scharf, J. Tiley, and R. Banerjee, Scripta Mater., 59, (2008) 487.
[8] A. Singh, J. Hwang, T.W. Scharf, J. Tiley, R. Banerjee," submitted to Composites Sci. Technol. (2008).
[9] R. Banerjee, A. Genç, D. Hill, P.C. Collins, H.L. Fraser, Scripta Mater. 53 (2005) 1433.
[10] R. Banerjee, P.C. Collins, D. Bhattacharyya, S. Banerjee, H.L. Fraser, Acta Mater. 51 (2003) 3277.
[11] H. Cai, F. Yan, Q. Xue, Mater. Sci. Eng. Struct. Mater. Properties Microstruct. Process. 364 (2004) 94.
[12] W.X. Chen, F. Li, G. Han, J.B. Xia, L.Y. Wang, J.P. Tu, Z.D. Xu, Tribol. Lett. 15 (2003) 275.
[13] R.W. Siegel, S.K. Chang, B.J. Ash, J. Stone, P.M. Ajayan, R.W. Doremus, L.S. Schadler, Scripta Mater. 44 (2001) 2061.

[14] G.D. Zhan, J.D. Kuntz, J.L. Wan, A.K. Mukherjee, Nat. Mater. 2 (2003) 38.
[15] J.P. Tu, L.P. Zhu, K. Hou, S.Y. Guo, Carbon 41 (2003) 1257.
[16] Z.H. Xia, J. Loub, W.A. Curtin, Scripta Mater. 58 (2008) 223.
[17] J.P. Tu, Y.Z. Yang, L.Y. Wang, X.C. Ma, X.B. Zhang, Tribol. Lett. 10 (2001) 225.
[18] W.X. Chen, J.P. Tu, L.Y. Wang, H.Y. Gan, Z.D. Xu, X.B. Zhang, Carbon 41 (2003) 215.
[19] J.P. Tu, L.P. Zhu, K. Hou, S.Y. Guo, Carbon 41 (2003) 1257.
[20] X.H. Chen, C.S. Chen, H.N. Xiao, H.B. Liu, L.P. Zhou, S.L. Li. G. Zhang, Trib. Int. 39 (2006) 22.
[21] K.T. Kim, S.I. Cha, S.H. Hong, Mat. Sci. Eng. A 449–451 (2007) 46.
[22] P.-Q. Dai, W.C. Xu, Q.-Y. Huang, Mat. Sci. Eng. A 483–484 (2008) 172.
[23] F.P. Bowden, D. Tabor, The Friction and Lubrication of Solids, Clarendon, Oxford, 1986, Part 1, p. 112.
[24] M. Godet, Wear 100, (1984) 437.
[25] Y. Bethier, M. Godet, and M. Brendle, Tribol. Trans. 32, (1989) 490.
[26] Y. Berthier, The Third Body Concept, Elsevier, Oxford, 1996, p. 21.
[27] I. L. Singer, S. D. Dvorak, K. J. Wahl, and T. W. Scharf, J. Vac. Sci. Technol. A 21, (2003) S232.
[28] S. Samuel, S. Nag, T.W. Scharf, R. Banerjee, Mat. Sci. Eng. C 28 (2008) 414.
[29] D. L. A. de Faria, S. Venaüncio Silva, M. T. de Oliveira, J. Raman Spect. 28, (1997) 873.
[30] R. Bhattacharya, G. Jha, S. Kundu, R. Shankar, N. Gope, Surf. Coat. Technol. 201 (2006) 526.
[31] K. Behler, S. Osswald, H. Ye, S. Dimovski, Y. Gogotsi, J. Nanoparticle Res. 8 (2006) 615.
[32] A.C. Ferrari, Solid State Commun. 143 (2007) 47.
[33] T.W. Scharf, R.D. Ott, D. Yang, and J.A. Barnard, J. Appl. Phys., 85 (1999) 3142.
[34] J. Huiming, A. Felix, M. Aroyave, Plasma Science and Technology, 10 (2008).

Figure Captions

Fig. 1. As-synthesized Ni-CNT nanocomposite (a) SEM image and (b) corresponding Auger electron spectroscopy map (256x256 pixels) showing distribution of CNT in Ni matrix. Green=Ni and Red=C.

Fig 2. Ni-CNT nanocomposite interface (a) SEM image and corresponding Auger electron spectroscopy maps (256x256 pixels) of (b) Ni, (c) C and (d) O. The thermal pseudocolor images show relative amounts of the constituents.

Fig 3. Coefficient of friction (COF) versus cycle curves for pure Ni and Ni-CNT nanocomposite tested against (a) 440C stainless steel counterface with P_{max}=0.6 GPa and (b) Si_3N_4 counterface with P_{max}=0.8 GPa.

Fig. 4. (a) Pure Ni and (c) Ni-CNT nanocomposite blended images of Raman spectroscopy color map and optical micrograph taken inside the wear tracks from friction tests in Fig. 3(a). Also shown are corresponding (b) and (d) Raman spectra taken inside (red circles and spectra) and outside (blue circles and spectra) the wear tracks. The blue circle in (d) shows the location of an unworn CNT. A reference Raman spectrum of CNT powder in (d) is shown for comparison. See text for further details.

Fig. 5. (a) Pure Ni and (c) Ni-CNT nanocomposite blended images of Raman spectroscopy color map and optical micrograph taken inside the wear tracks from friction tests in Fig. 3(b). Also shown are corresponding (b) and (d) Raman spectra taken inside (red circles and spectra) and outside (blue circles and spectra) the wear tracks. The blue circle in (d) shows the location of an unworn CNT. A reference Raman spectrum of CNT powder in (d) is shown for comparison. See text for further details.

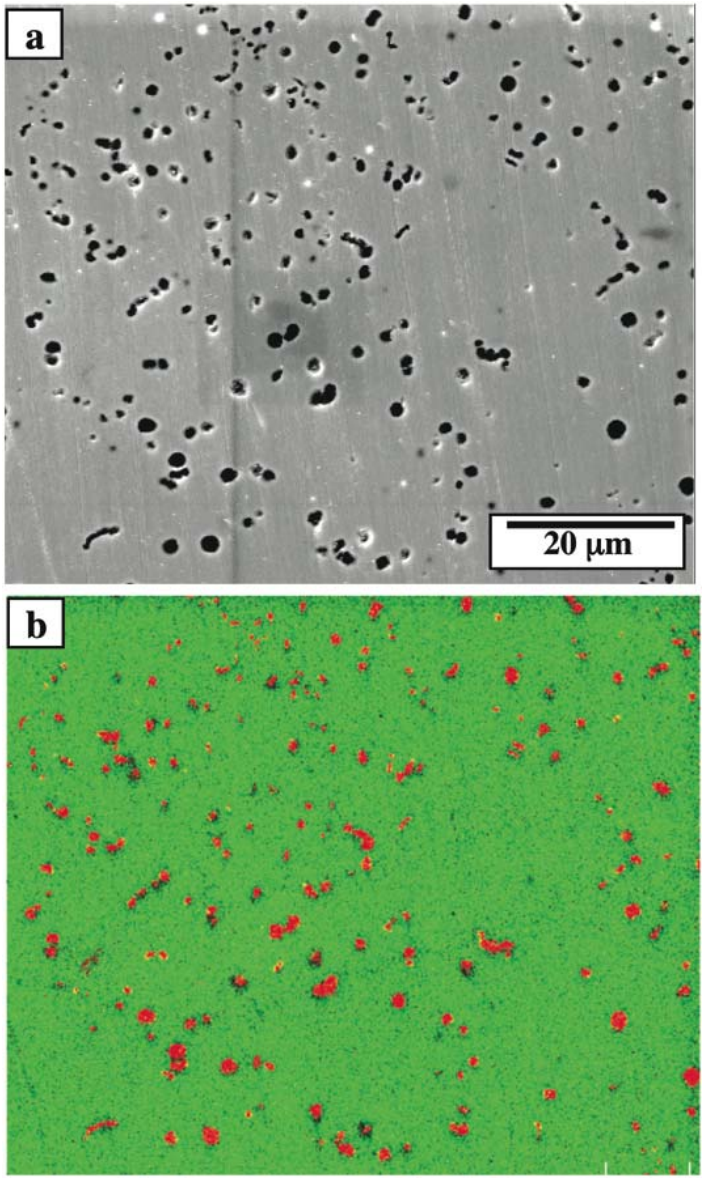

Fig. 1.

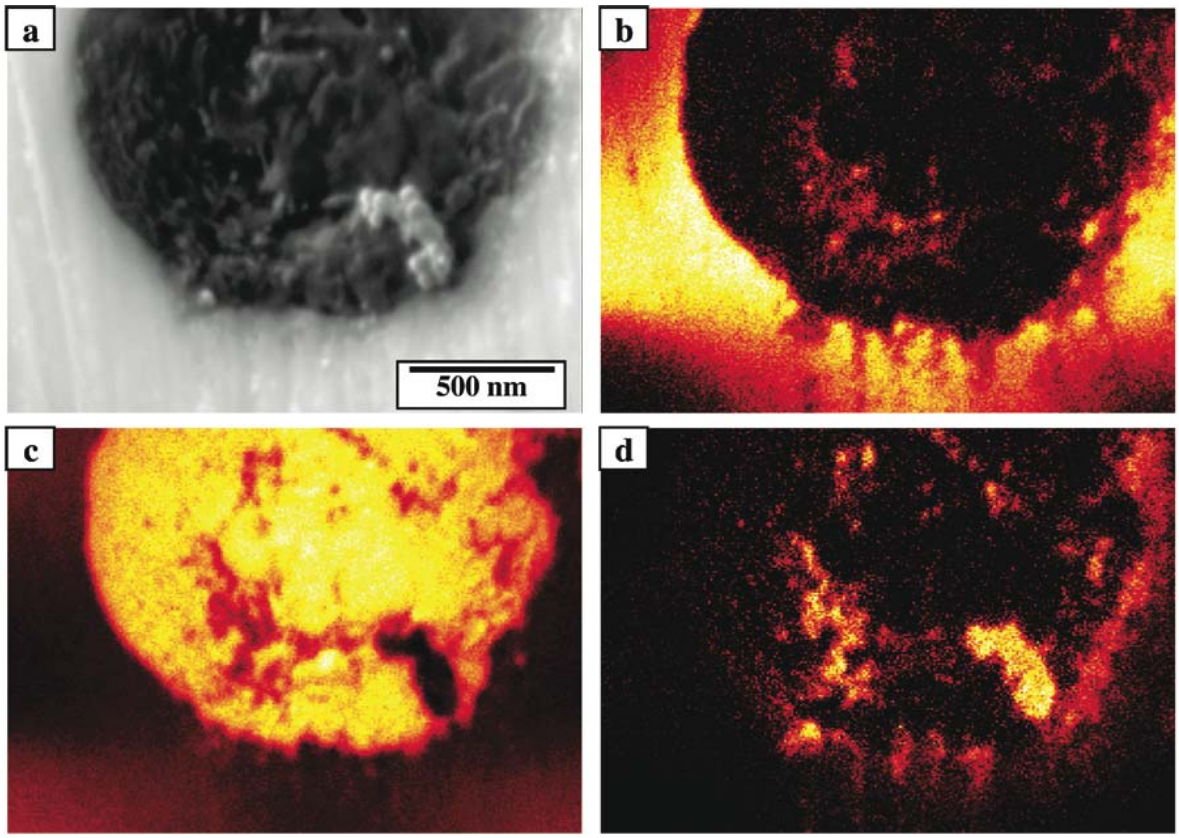

Fig. 2.

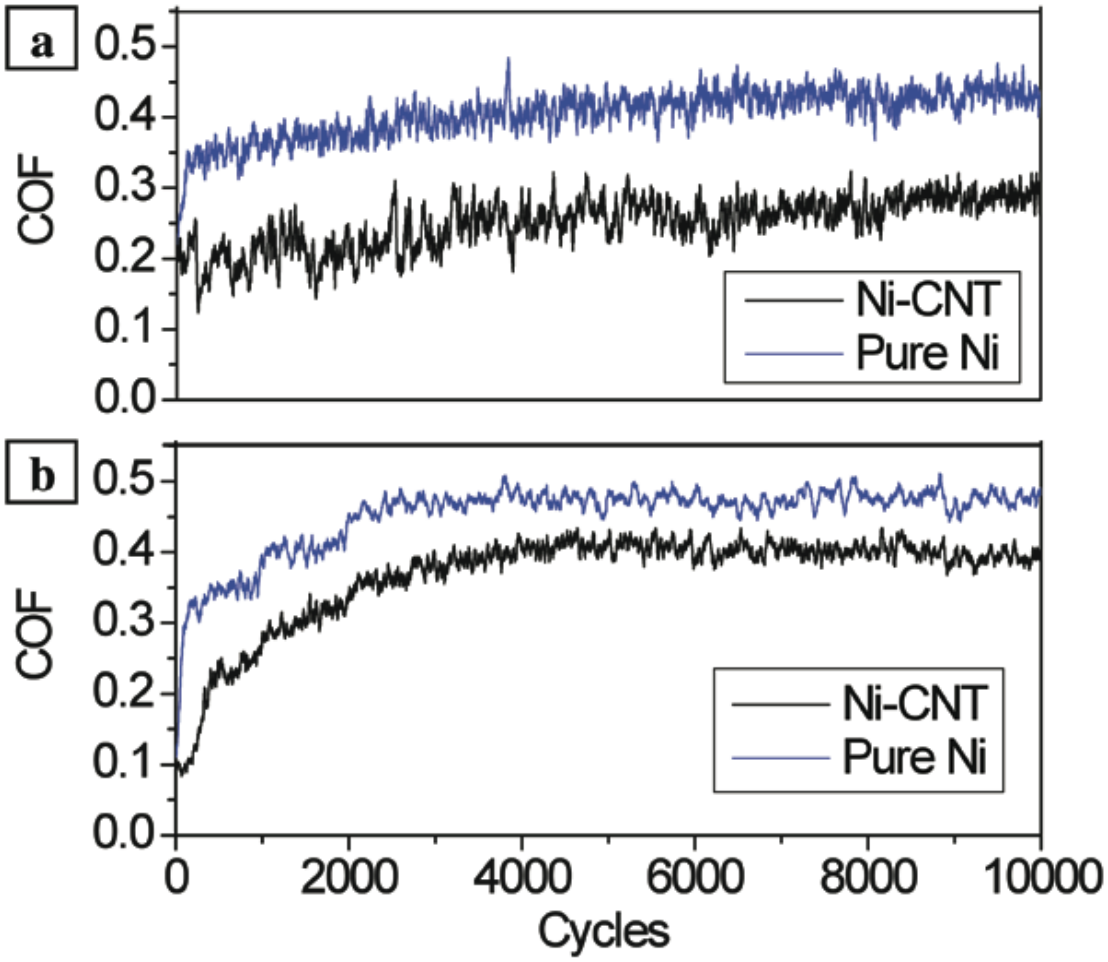
a
b
COF
COF
0.0
0.1
0.2
0.3
0.4
0.5
0
2000
4000
6000
8000
10000
Cycles
Ni-CNT
Pure Ni
Ni-CNT
Pure Ni

Fig. 3.

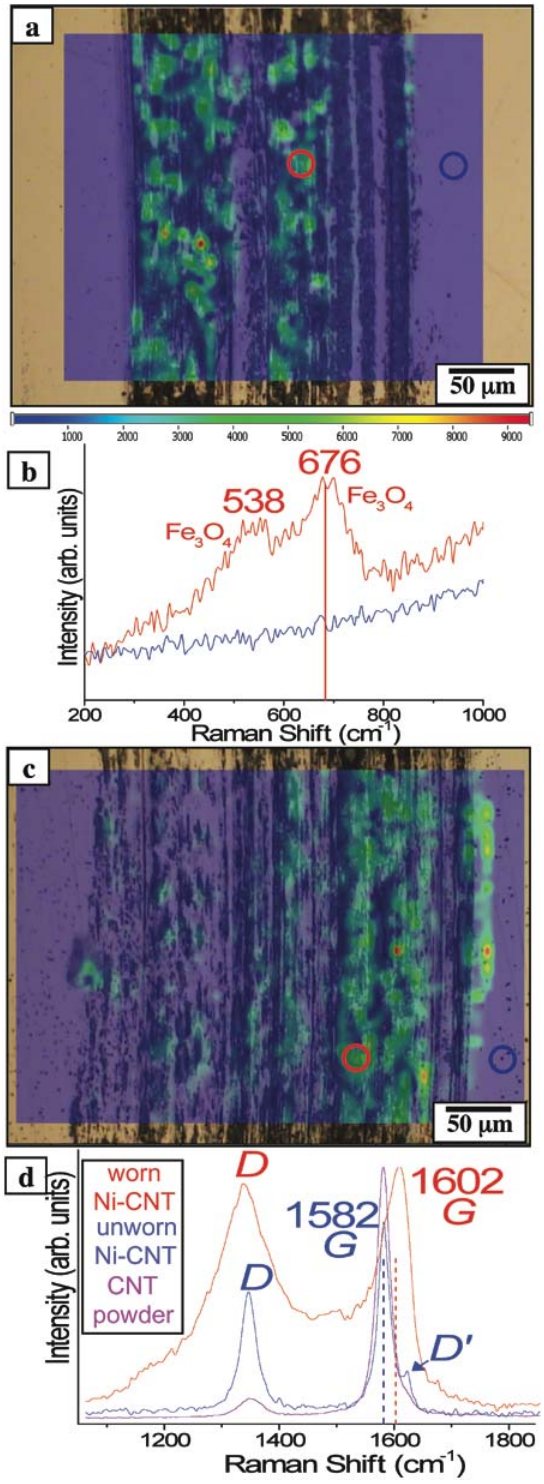
a
50 μm
1000
2000
3000
4000
5000
6000
7000
8000
9000
b
676
538
Fe_3O_4
Fe_3O_4
Intensity (arb. units)
200
400
600
800
1000
Raman Shift (cm^{-1})
c
50 μm
d
worn
Ni-CNT
unworn
Ni-CNT
CNT
powder
D
1582
G
1602
G
D
D'
Intensity (arb. units)
1200
1400
1600
1800
Raman Shift (cm^{-1})

Fig. 4.

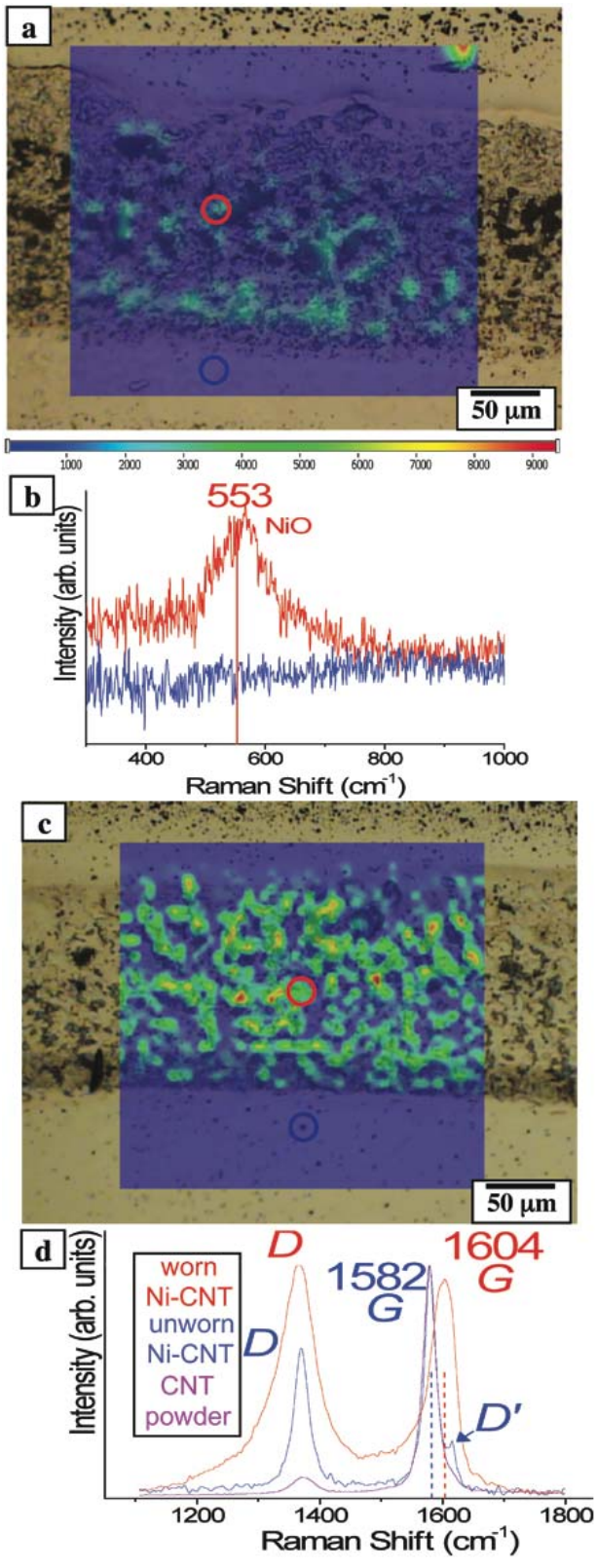
a
50 µm
1000
2000
3000
4000
5000
6000
7000
8000
9000
b
553
NiO
Intensity (arb. units)
400
600
800
1000
Raman Shift (cm-1)
c
50 µm
d
worn
Ni-CNT
unworn
Ni-CNT
CNT
powder
D
1582
G
1604
G
D
D'
Intensity (arb. units)
1200
1400
1600
1800
Raman Shift (cm-1)

Fig. 5.